

# Identically Sized Co Quantum Dots on Monolayer WS<sub>2</sub> Featuring Ohmic Contact

Weiqing Tang, Mingming Fu, Jiajun Chen, Baofan Sun, Congming Ke, Yaping Wu,<sup>\*</sup> Xu Li, Chunmiao Zhang, Zhiming Wu,<sup>†</sup> and Junyong Kang

*Department of Physics, OSED, Fujian Provincial Key Laboratory of Semiconductor Materials and Applications, Xiamen University, Xiamen 361005, China*



(Received 6 September 2019; revised manuscript received 1 December 2019; accepted 14 January 2020; published 4 February 2020)

Identically sized Co quantum dots (QDs) are constructed on monolayer tungsten disulfide (WS<sub>2</sub>), forming coupled heterostructures. Topographical images investigated by means of *in situ* scanning tunneling microscopy (STM) show a bias-dependent feature. First-principles-calculated binding energies combined with the simulated STM images identify that the Co QDs possess a unique magic number, with a tetrahedral Co<sub>4</sub> configuration. Numerical differential conductance measured by means of scanning tunneling spectroscopy indicates a *p*-type doping and an Ohmic contact property for the Co<sub>4</sub>/WS<sub>2</sub> system. The mechanism of the transport and conduction properties of the coupled heterostructures is further revealed by analyzing the work functions and interfacial interaction. Our findings offer some references for the controlled fabrication of identically sized zero-dimensional and two-dimensional heterostructures, and we propose a feasible strategy for Ohmic interface contact in nanodevices.

DOI: 10.1103/PhysRevApplied.13.024003

## I. INTRODUCTION

The fabrication of heterostructures with different dimensions offers tunable ways, beyond the limit of size and shape, to regulate the electronic properties of materials [1–10]. The discovery of two-dimensional (2D) materials opens up a new paradigm for the integration of nanoscale material and enables optoelectronic applications due to their atomic-scale thickness and various band structures [11–16]. As a kind of semiconducting material, transition-metal dichalcogenides (TMDCs) possess tunable band gaps, ranging from ultraviolet to infrared, that allow a large control degree for multiple functional devices [3,5,6]. Because of the strong spin-orbit interaction and inversion symmetry breaking, individual monolayer (ML) TMDCs show spin-valley coupling and valley-contrasting physical properties, which are also expected to be unique features for the design of highly efficient spin-optoelectronic devices [17,18]. In addition to 2D materials, zero-dimensional (0D) nanomaterials, such as plasmonic nanoparticles and quantum dots (QDs), exhibit intrinsic advantages of a strong size-confined effect, large specific surface areas, and short charge-transfer lengths [19,20]. They provide a platform for investigating fascinating physical phenomena on the quantum scale that are essentially different from those of traditional bulk materials. The integration of 2D TMDC materials with 0D nanostructures

to form 0D and 2D heterostructures thus attracts considerable interest. In particular, if combining 3d transition-metal (TM) nanostructures with monolayer TMDCs, magnetic interactions through the proximity effect may allow a spin-valley modulation in monolayer TMDCs. Hence, the 0D and 2D heterostructures can be promising candidates for spintronic applications, such as ultrahigh-density magnetic memory.

Consistent performances of 0D and 2D devices require 0D nanostructures with uniform shape and size. Despite the periodically regular lattices of 2D TMDCs, the absence of a surface dangling bond is not conducive for bearing the thermal perturbation to form identically sized nanostructures. Currently, some 0D nanostructures, such as Fe and Pt nanoparticles [21,22], with different morphologies and various coverage, have been successfully fabricated on MoS<sub>2</sub> film; however, identically sized magnetic nanostructures on monolayer TMDCs have not been reported, so far. Apart from controlled fabrication, interfacial interactions, especially between metal and semiconductor materials, are another issue of concern that determines the device performance. How to form an Ohmic contact in a metal-semiconductor is a significant topic for device fabrication. However, work-function differences and dangling-bond-free surfaces of TMDCs make it hugely challenging to form low-resistance metal contacts with 2D TMDCs [23]. Though theoretical studies have demonstrated that van der Waals (vdW) interactions in the interface can be eliminated by selecting a specific metal [24], Ohmic contact of semiconductor-metal heterostructures has scarcely been

<sup>\*</sup>ypwu@xmu.edu.cn

<sup>†</sup>zwmw@xmu.edu.cn

reported in experiments. In principle, work functions of metals can be changed by adjusting their shape and size [25]. Constructing metal nanostructures with specific configurations may be a feasible strategy to reduce the contact barrier, and thus, improve the electronic performance of the devices. Hence, fabricating integrated heterostructures with 0D ferromagnetic metal TMs and 2D TMDCs to ascertain the geometrical and electronic structures, and reveal the interfacial interactions of the system, are of significant importance.

Here, identically sized Co QDs are grown in a controlled manner on monolayer WS<sub>2</sub>, forming coupled heterostructures. *In situ* scanning tunneling microscopy (STM) is employed to characterize the morphologies and electronic structures systematically at both positive and negative bias voltages. Based on the binding energies of various structures derived from first-principles calculations, the experimental atomic configuration of Co QDs is identified. The numerical differential conductance ( $dI/dV-V$ ) spectra are studied by means of scanning tunneling spectroscopy (STS), which reveal an Ohmic contact in our Co/WS<sub>2</sub> system. The modulated work functions of Co QDs and interfacial interactions are analyzed to explain the transport and conduction properties of the coupled Co/WS<sub>2</sub> heterostructures.

## II. METHODS AND CHARACTERIZATION

High-quality monolayer WS<sub>2</sub> is synthesized on SiO<sub>2</sub>/Si substrates using the chemical vapor deposition (CVD) method and then transferred to Au sheets through a standard transfer process [26]. The monolayer WS<sub>2</sub> is annealed under ultrahigh vacuum (UHV) conditions at 473 K for 12 h to achieve a clean surface. High-purity Co (99.999%) is evaporated from a tantalum boat at a rate of about 0.141 ML/min (1 ML =  $6.6 \times 10^{13}$  Co atoms/cm<sup>2</sup>) and about 0.154 ML Co atoms are deposited *in situ* onto WS<sub>2</sub> at a substrate temperature of about 100 K. All STM images are measured using chemically etched tungsten tips in constant-current mode at a cryogenic temperature of about 78 K and a base pressure of about  $6 \times 10^{-11}$  torr. Spectroscopic measurements are recorded by using the standard lock-in technique. A modulation signal of 10 mV peak-to-peak at 957 Hz is added to the dc sample bias to obtain the  $dI/dV$  data.

The first-principles calculations are performed by using density functional theory (DFT), as implemented in the Vienna *ab initio* simulation package (VASP) code with the projector augmented wave (PAW) pseudopotential [27]. The exchange-correlation effects are treated by the generalized gradient approximation (GGA) in the form proposed by Perdew-Burke-Ernzerhof (PBE) [28]. The periodic slab models include one layer of  $5 \times 5$  unit cells of WS<sub>2</sub>, Co QDs with various configurations, and a vacuum layer of 25 Å. The 2D Brillouin zone (BZ) is sampled with a

$7 \times 7 \times 1$  Monkhorst-Pack grid of  $k$  points. The cutoff energy and convergence criteria for Hellmann–Feynman forces and total energy are set to 364 eV, 0.01 eV Å<sup>-1</sup>, and 10<sup>-4</sup> eV, respectively.

## III. RESULTS AND DISCUSSION

An atom-resolved empty-state STM image of monolayer WS<sub>2</sub> is shown in Fig. 1(a). Pristine WS<sub>2</sub> exhibits long-range-ordered 2D lattices with honeycomblike structures. One set of hexagonally arranged 2D fast Fourier transform (FFT) spots confirms the high crystal quality of the grown monolayer WS<sub>2</sub>. The period of atomic corrugation is measured to be 3.17 Å, which is consistent with previous reports [5]. Several STS spectra taken at different positions on monolayer WS<sub>2</sub> are shown in Fig. 1(b). The valence band maximum (VBM) and conduction band minimum (CBM), denoted by dashed black lines, are located at -1.51 and 0.16 eV, respectively, defining a band gap of about 1.67 eV. Notably, the measured band gap is smaller than that of general monolayer WS<sub>2</sub> [29]. This is because of electron donation from the Au substrate to monolayer WS<sub>2</sub>, which is even enhanced after annealing pretreatment and contributes to the valence band maximum of WS<sub>2</sub> [29]. Asymmetrical locations of the VBM and CBM suggest an *n*-type semiconducting property. After Co deposition, a series of filled- and empty-state STM images are taken at

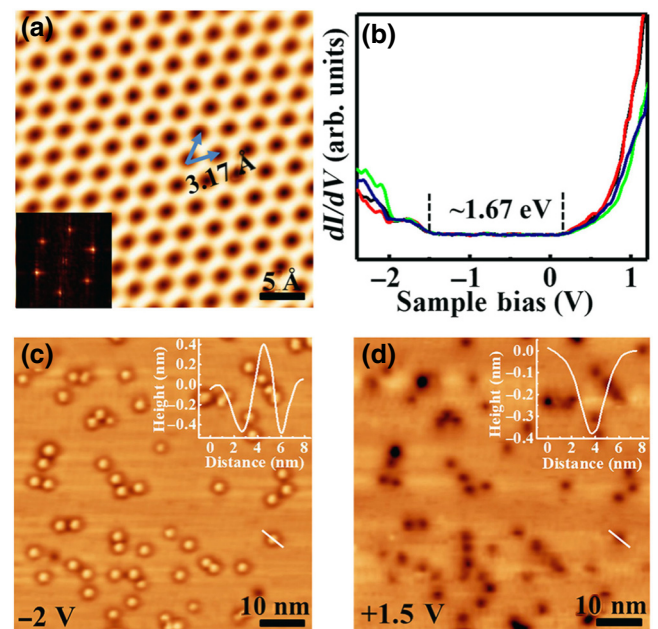


FIG. 1. (a) STM image ( $V_s = +1.7$  V,  $I_s = 570$  pA) and (b) normalized STS spectra ( $V_s = +1.4$  V,  $I_s = 200$  pA,  $V_{rms} = 10$  mV,  $f = 975$  Hz) of monolayer WS<sub>2</sub>. Filled- and empty-state STM images of 0.154 ML Co atoms on monolayer WS<sub>2</sub> recorded at (c)  $V_s = -2.0$  V,  $I_s = 500$  pA, and (d)  $V_s = +1.5$  V,  $I_s = 550$  pA.

different bias voltages to investigate the surface morphologies and electronic states, as shown in Figure S1 within the Supplemental Material [30]. It is clearly seen that the morphology is sensitive to the polarity of voltages, but hardly changes when varying the voltage values. Figures 1(c) and 1(d) are typical STM images of filled and empty states, respectively, and the height profiles along Co QDs are displayed in the insets. As shown in Fig. 1(c), the Co atoms form identically sized QDs, which distribute randomly on monolayer WS<sub>2</sub>. The Co QDs are exhibited as bright dots with a measured height and lateral size of about 0.4 nm and 3 nm, respectively. As the voltage changes to positive values, the height is seriously suppressed, leaving only dark dots decorating the surface [seeing Fig. 1(d)]. More interestingly, the QDs can steadily exist, even as the temperature rises to room temperature, as shown in Figure S2 within the Supplemental Material [30]. In addition, we make a series of measurements to exclude the influence of point defects on the formation of QDs (see a detailed discussion within the Supplemental Material [30]). It is found that the observed identically sized Co QDs are not located above the point defects of WS<sub>2</sub>.

Given the identical sizes, the Co QD is considered to have a magic number [31]. To resolve the atomic structure, first-principles calculations are performed for the Co/WS<sub>2</sub> system. The optimized monolayer WS<sub>2</sub> in Fig. 2(a) shows a hexagonal honeycomb structure in the (0001) plane with

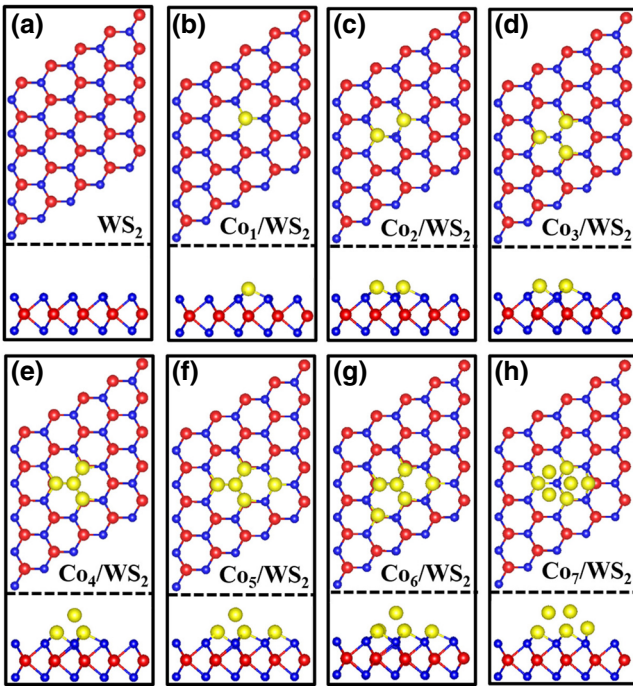


FIG. 2. Top and side views of the geometrical structures of pristine monolayer WS<sub>2</sub> and the most stable Co/WS<sub>2</sub> systems with one to seven Co atoms absorbed. The red, blue, and yellow spheres represent the W, S, and Co atoms, respectively.

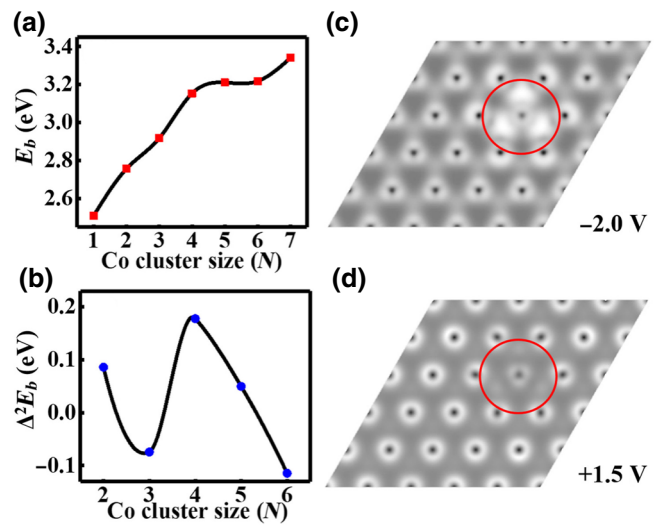


FIG. 3. (a) Binding energy per atom as a function of Co QDs size  $N$ . (b) Calculated stability function versus the number of Co atoms. Simulated STM images of Co<sub>4</sub>/WS<sub>2</sub> system at bias voltages of (c) −2.0 V and (d) +1.5 V.

a lattice constant of 3.19 Å, which is consistent with our experimental result. According to structural information provided by the STM images, possible configurations of Co <sub>$N$</sub>  ( $N$  denotes the number of adsorbed Co adatoms, ranging from 1 to 7) QDs are constructed on monolayer WS<sub>2</sub>, as seen in Figure S4 within the Supplemental Material [30]. For fixed configurations of the QDs, the binding energy per atom,  $E_b$ , is calculated from  $E_b = (E_{\text{WS}_2} + NE_{\text{Co}} - E_{\text{NCo/WS}_2})/N$  [28], where  $E_{\text{Co}}$ ,  $E_{\text{WS}_2}$ , and  $E_{\text{NCo/WS}_2}$  stand for the energies of the Co adatom, monolayer WS<sub>2</sub>, and Co <sub>$N$</sub> -absorbed WS<sub>2</sub> systems, respectively. Through the total energy comparison, the most stable configuration at each given size ( $N$ ) of Co QDs is revealed and displayed in Figs. 2(b)–2(h), and the size-dependent binding energy is shown in Fig. 3(a). The binding energy sharply increases with QD size until  $N = 4$ , then maintains relatively stable values in the range of  $N = 4$ –5, and finally rapidly reaches a maximum with  $N = 7$ . Since the magic number normally demonstrates the relative stability of a Co <sub>$N$</sub>  QD with respect to its neighboring sizes, Co <sub>$N-1$</sub>  and Co <sub>$N+1$</sub> , the second-derivative binding energy  $\Delta^2 E_b(N)$  (where  $\Delta^2 E_b(N) = 2E_b(N) - [E_b(N+1) + E_b(N-1)]$ ), which denotes the strength of a magic structure's stability [32,33], is plotted in Fig. 3(b) to explain the formation of the magic structure. The maximum value is present at  $N = 4$ , implying a magic number of four for the Co QDs. In the Co<sub>4</sub> QD, three Co atoms occupy the top site of neighboring W atoms and the remaining Co atom is located at the top site of the S atom, forming a pyramid structure. The morphology of Co<sub>4</sub> QD is consistent with the observed STM images, which also reasonably support the Co<sub>4</sub> configuration. In our experiments, we also observe a

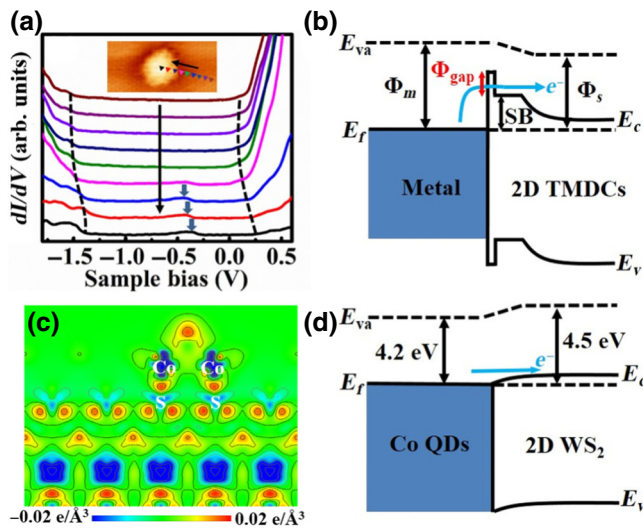


FIG. 4. (a) Normalized STS spectra recorded across Co QDs shown in the STM image (inset) (STM image:  $V_s = -1.5$  V,  $I_s = 500$  pA; STS spectra:  $V_s = 1.5$  V,  $I_s = 200$  pA). Proposed band diagram of (b) metal/2D TMDCs and (d) Co<sub>4</sub>/WS<sub>2</sub> interface. (c) Differential charge densities of the Co<sub>4</sub>/WS<sub>2</sub> system. SB is the Schottky barrier.

few QDs that are smaller or larger than Co<sub>4</sub> QDs. Through a statistical calculation at different regions, the populations of the smaller and larger QDs are approximately 6% and 8%, respectively. By comparing the calculated partial charge densities and the observed images, some smaller QDs with  $N = 3$  and larger QDs with  $N = 5$  may be distinguished, however, their populations are much lower than that of  $N = 4$  (see a detailed discussion within the Supplemental Material [30]). The calculated total magnetic moment, induced magnetic moment of WS<sub>2</sub>, and magnetic anisotropy energy (MAE) of Co<sub>4</sub>/WS<sub>2</sub> systems are  $4 \mu_B$ ,  $0.04 \mu_B$ , and  $-0.17$  meV, respectively. The ferromagnetic coupling among Co atoms and between Co<sub>4</sub> and WS<sub>2</sub> could further stabilize the Co<sub>4</sub> configuration, which basically remains unchanged, even at room temperature.

To explain the voltage-dependent STM morphology, filled- and empty-state STM images of the Co<sub>4</sub>/WS<sub>2</sub> system are simulated through VASP software using the Tersoff and Hamann theory [34], as shown in Figs. 3(c) and 3(d). At the filled-state voltage of  $-2.0$  V, the electronic states accumulate on the Co<sub>4</sub> nanoclusters and are stronger than the states of the WS<sub>2</sub> substrate [red circle in Fig. 3(c)], resulting in bright contrast of Co<sub>4</sub> nanoclusters in the STM image. In contrast, the electronic states of Co<sub>4</sub> nanoclusters for the empty state are weaker than that of WS<sub>2</sub> [red circle in Fig. 3(d)] at a voltage of  $+1.5$  V, which agrees well with the experimental observation in positive voltage. A similar phenomenon has been measured in alkali metals adsorbed on MoS<sub>2</sub> and MoSe<sub>2</sub> by STM at positive bias [35].

To gain a deeper insight into the interfacial interaction and transport properties, STS measurements are performed

on various positions around a Co<sub>4</sub> QD and on monolayer WS<sub>2</sub> for comparison, as shown in Fig. 4(a). When measuring the WS<sub>2</sub> surface at a 1 nm lateral distance away from the Co<sub>4</sub> QD, the  $dI/dV$  curve exhibits typical electronic properties of intrinsic monolayer WS<sub>2</sub>. Upon getting close to the Co<sub>4</sub> QD, the Fermi level ( $E_F$ ) downshifts toward the VBM, which implies *p*-type doping. A delocalized acceptor state appears at about  $-0.4$  eV in the gap, as indicated by the blue arrow, which is attributed to the doping effect from the Co<sub>4</sub> QD. As the tip moves more closely to the center of the Co<sub>4</sub> QD, the acceptor state shifts to higher energy with slightly increased intensity and contributes to the bright protrusions detected under negative-bias conditions. Meanwhile, the distribution of electronic states at positive voltages gradually decays, which results in the observed dark states of the Co<sub>4</sub> QDs at positive sample bias.

More interestingly, the value of the band gap basically remains unchanged compared with that of pristine monolayer WS<sub>2</sub>, which exhibits Ohmic character, rather than behaving as a typical Schottky contact. As we know, the non-Ohmic contact can generally induce additional resistance in metal-semiconductor heterostructures, resulting in an enlarged band gap [24,36]. The band gap of Co<sub>4</sub>/WS<sub>2</sub> is essentially consistent with that of monolayer WS<sub>2</sub>, which implies that the additional resistance does not exist in the electronic structure of the heterostructures and Ohmic contact is formed at the interface. In addition, it is well known that the SB is normally present in the contact interface, if the work function of the metal is larger than that of the *n*-type semiconductor materials. By employing the work functions of bulk Co ( $\sim 5$  eV) and monolayer WS<sub>2</sub> ( $\sim 4.5$  eV) [37], a Schottky barrier of about 0.5 eV should be expected. Further considering the dangling-bond-free surface, an additional van der Waals barrier ( $\Phi_{gap}$ ) may also exist before the inherent Schottky barrier in the interface, as schematically drawn in Fig. 4(b) [23,24]. However, in view of the invariable band gap in our STS results, the Schottky barrier is barely present. The internal mechanism can be attributed to the size effect of Co QDs. As demonstrated in Ref. [25], metals with nanostructures possess smaller work functions than that of the bulk due to the size effect. To address this issue, work functions of both Co<sub>4</sub> QDs and Co bulk are calculated and compared. The results show that the work function of Co<sub>4</sub> QDs (4.2 eV) is notably smaller than that of Co bulk (4.9 eV). The value is even smaller than that of monolayer WS<sub>2</sub> (4.5 eV), contributing to the Ohmic contact instead of the normal Schottky barrier between Co<sub>4</sub> QDs and monolayer WS<sub>2</sub>. Except for the reduction of work functions, differential charge densities of the Co<sub>4</sub>/WS<sub>2</sub> system are calculated to analyze the interface interaction, as illuminated in Fig. 4(c). The negative charge densities are observed to accumulate around the Co and S atoms, while the positive charge densities are shared by neighboring Co and S atoms to form Co—S bonds. This kind of charge

distribution is a typical characteristic of a covalent interaction, which eliminates the van der Waals barrier in the interface [38,39]. In the light of this, by constructing identically sized  $\text{Co}_4$  QDs, both the general Schottky and van der Waals barriers are avoided, and an Ohmic contact is demonstrated in the  $\text{Co}_4/\text{WS}_2$  interface, as shown in Fig. 4(d).

It is also noticed that the detected electronic states at positive voltages show a certain decay trend, which can be attributed to the effective potential,  $V_{\text{eff}}$ , of electrons.  $V_{\text{eff}} = V_{\text{xc}} + V_H + V_{\text{ext}}$  suggests the interaction of transport electrons with other electrons and the external electrostatic field, where  $V_{\text{xc}}$  is the exchange-correlation potential originating from the quantum mechanical nature of the electrons,  $V_H$  denotes the Hartree potential because of the mean-field electrostatic interactions, and  $V_{\text{ext}}$  is other electrostatic interactions in the system [24].

#### IV. CONCLUSION

Co QDs with identical sizes are successfully fabricated on monolayer  $\text{WS}_2$ . *In situ* STM measurements show a bias-dependent feature. Binding energies and simulated STM images reveal the unique magic number and tetrahedral configuration of  $\text{Co}_4$  QDs. The *p*-type doping property and delocalized gap state are detected by STS, which result in the measured bright states under negative-bias conditions. Weakened electric states of the CBM lead to the measured dark image under positive-bias conditions. Ohmic interface contact is exhibited in the invariable band gap in the STS results. The size-dependent work function and covalent interaction between  $\text{Co}_4$  and monolayer  $\text{WS}_2$  are found to be responsible for the transport and conduction properties of the coupled heterostructures. All results in this work suggest a route for developing identically sized 0D and 2D heterostructure nanodevices toward an Ohmic-contacted interface, which is critical for the future applications of nanoelectronics.

#### ACKNOWLEDGMENTS

The work is supported by the National Key Research and Development Program of China (Grant No. 2016YFB0400801 and No. 2018YFB0406603), the National Natural Science Foundations of China (Grants No. 61774128, No. 61874092, No. 61674124, No. 61974125, No. 11604275, No. 61704040, and No. 61804129), the Natural Science Foundation of Fujian Province of China (Grants No. 2018I0017 and No. 2017J01012), and the Fundamental Research Funds for the Central Universities (Grants No. 20720190055 and No. 20720190058).

[1] A. Barla, V. Bellini, S. Rusponi, P. Ferriani, M. Pivetta, F. Donati, F. Patthey, L. Persichetti, S. K. Mahatha,

- M. Papagno, C. Piamonteze, S. Fichtner, S. Heinze, P. Gambardella, H. Brune, and C. Carbone, Complex magnetic exchange coupling between Co nanostructures and Ni (111) across epitaxial graphene, *ACS Nano* **10**, 1101 (2016).
- [2] G. Cheng, B. Li, C. Zhao, X. Yan, H. Wang, K. M. Lau, and J. Wang, Interfacially bound exciton state in a hybrid structure of monolayer  $\text{WS}_2$  and InGaN quantum dots, *Nano Lett.* **18**, 5640 (2018).
- [3] Y.-H. Chu, L.-H. Wang, S.-Y. Lee, H.-J. Chen, P.-Y. Yang, C. J. Butler, L.-S. Lu, H. Yeh, W.-H. Chang, and M.-T. Lin, Atomic scale depletion region at one dimensional  $\text{MoSe}_2$ - $\text{WSe}_2$  heterointerface, *Appl. Phys. Lett.* **113**, 241601 (2018).
- [4] T. Eelbo, M. Waśniowska, M. Gyamfi, S. Forti, U. Starke, and R. Wiesendanger, Influence of the degree of decoupling of graphene on the properties of transition metal adatoms, *Phys. Rev. B* **87**, 205443 (2013).
- [5] H. M. Hill, A. F. Rigos, K. T. Rim, G. W. Flynn, and T. F. Heinz, Band alignment in  $\text{MoS}_2$ / $\text{WS}_2$  transition metal dichalcogenide heterostructures probed by scanning tunneling microscopy and spectroscopy, *Nano Lett.* **16**, 4831 (2016).
- [6] A. Mushtaq, S. Ghosh, A. S. Sarkar, and S. K. Pal, Multiple exciton harvesting at zero-dimensional/two-dimensional heterostructures, *ACS Energy Lett.* **2**, 1879 (2017).
- [7] Y. Pan, S. Fölsch, Y.-C. Lin, B. Jariwala, J. A. Robinson, Y. Nie, K. Cho, and R. M. Feenstra,  $\text{WSe}_2$  homojunctions and quantum dots created by patterned hydrogenation of epitaxial graphene substrates, *2D Mater.* **6**, 021001 (2019).
- [8] J. Ren, H. Guo, J. Pan, Y. Y. Zhang, X. Wu, H. G. Luo, S. Du, S. T. Pantelides, and H. J. Gao, Kondo effect of cobalt adatoms on a graphene monolayer controlled by substrate-induced ripples, *Nano Lett.* **14**, 4011 (2014).
- [9] K. R. Williams, B. T. Diroll, N. E. Watkins, X. Rui, A. Brumberg, R. F. Klie, and R. D. Schaller, Synthesis of type I  $\text{PbSe}/\text{CdSe}$  Dot-on-plate heterostructures with near-infrared emission, *J. Am. Chem. Soc.* **141**, 5092 (2019).
- [10] J. Wyrick, F. D. Natterer, Y. Zhao, K. Watanabe, T. Taniguchi, W. G. Cullen, N. B. Zhitenev, and J. A. Stroscio, Tomography of a probe potential using atomic sensors on graphene, *ACS Nano* **10**, 10698 (2016).
- [11] Y. Zhang, X. L. Sui, D. L. Ma, K. K. Bai, W. H. Duan, and L. He, Spin-Polarized Semiconducting Band Structure of Monolayer Graphene on Ni(111), *Phys. Rev. Appl.* **10**, 054043 (2018).
- [12] H. L. Zheng, B. S. Yang, D. D. Wang, R. L. Han, X. B. Du, and Y. Yan, Tuning magnetism of monolayer  $\text{MoS}_2$  by doping vacancy and applying strain, *Appl. Phys. Lett.* **104**, 132403 (2014).
- [13] B. Naydenov, S. Torsney, A. S. Bonilla, A. Gualandi, L. Mengozzi, P. G. Cozzi, R. Gutierrez, G. Cuniberti, and J. J. Boland, Mapping Conformational Changes in a Self-Assembled Two-Dimensional Molecular Network by Statistical Analysis of Conductance Images, *Phys. Rev. Appl.* **11**, 034070 (2019).
- [14] C. Zhang, Y. Wu, Y. Zhou, N. Gao, F. Guo, X. Chen, B. Jiang, W. Hu, and J. Kang, Two-dimensional Au lattices featuring unique carrier transport preference and wide forbidden gap, *Nanoscale* **6**, 10118 (2014).

- [15] S. Y. Li, K. K. Bai, W. J. Zuo, Y. W. Liu, Z. Q. Fu, W. X. Wang, Y. Zhang, L. J. Yin, J. B. Qiao, and L. He, Tunneling Spectra of a Quasifreestanding Graphene Monolayer, *Phys. Rev. Appl.* **9**, 054031 (2018).
- [16] Y. Cao, Z. J. Wang, Q. Bian, Z. W. Cheng, Z. B. Shao, Z. Y. Zhang, H. G. Sun, X. Zhang, S. J. Li, H. Gedeon, L. j. Liu, X. N. Wang, H. Yuan, and M. H. Pan, Phonon modes and photonic excitation transitions of MoS<sub>2</sub> induced by top-deposited graphene revealed by Raman spectroscopy and photoluminescence, *Appl. Phys. Lett.* **114**, 133103 (2019).
- [17] J. Schaibley, H. Y. Yu, G. Clark, P. Rivera, J. S. Ross, K. L. Seyler, W. Yao, and X. D. Xu, Valleytronics in 2D materials, *Nat. Rev. Mater.* **1**, 1 (2016).
- [18] H. Y. Yu, X. D. Cui, X. D. Xu, and W. Yao, Valley excitons in two-dimensional semiconductors, *Natl. Sci. Rev.* **2**, 57 (2015).
- [19] X. Dai, Z. Zhang, Y. Jin, Y. Niu, H. Cao, X. Liang, L. Chen, J. Wang, and X. Peng, Solution-processed, high-performance light-emitting diodes based on quantum dots, *Nature* **515**, 96 (2014).
- [20] A. P. Alivisatos, Semiconductor QDs, nanocrystals, and quantum dots, *Science* **271**, 933 (1996).
- [21] S. Wang, H. Sawada, X. Han, S. Zhou, S. Li, Z. X. Guo, A. I. Kirkland, and J. H. Warner, Preferential Pt nanocluster seeding at grain boundary dislocations in polycrystalline monolayer MoS<sub>2</sub>, *ACS Nano* **12**, 5626 (2018).
- [22] H. C. Hsu, C. B. Wu, K. L. Hsu, P. C. Chang, T. Y. Fu, V. R. Mudinepalli, and W. C. Lin, Surface morphology, magnetism and chemical state of Fe coverage on MoS<sub>2</sub> substrate, *Appl. Surf. Sci.* **357**, 551 (2015).
- [23] A. Allain, J. H. Kang, K. Banerjee, and A. Kis, Electrical contacts to two-dimensional semiconductors, *Nat. Mater.* **14**, 1195 (2015).
- [24] J. H. Kang, W. Liu, D. Sarkar, D. Jena, and K. Banerjee, Computational Study of Metal Contacts to Monolayer Transition-Metal Dichalcogenide Semiconductors, *Phys. Rev. X* **4**, 031005 (2014).
- [25] Y. P. Wu, W. Jiang, Y. J. Ren, W. W. Cai, W. H. Lee, H. F. Li, R. D. Piner, C. W. Pope, Y. F. Hao, H. X. Ji, J. Y. Kang, and R. S. Ruoff, Tuning the doping type and level of graphene with different gold configurations, *Small* **8**, 3129 (2012).
- [26] J. J. Chen, K. Shao, W. H. Yang, W. Q. Tang, J. P. Zhou, Q. M. He, Y. P. Wu, C. M. Zhang, X. Li, X. Yang, Z. M. Wu, and J. Y. kang, Synthesis of wafer-scale monolayer WS<sub>2</sub> crystals toward the application in integrated electronic devices, *ACS Appl. Mater. Inter.* **11**, 19381 (2019).
- [27] C. M. Ke, Y. P. Wu, G.-Y. Guo, W. Lin, Z. M. Wu, C. J. Zhou, and J. Y. Kang, Tuning the Electronic, Optical, and Magnetic Properties of Monolayer GaSe with a Vertical Electric Field, *Phys. Rev. Appl.* **9**, 044029 (2018).
- [28] W. Q. Tang, C. M. Ke, M. M. Fu, Y. P. Wu, C. M. Zhang, W. Lin, S. Q. Lu, Z. M. Wu, W. H. Yang, and J. Y. Kang, Electrically tunable magnetic configuration on vacancy-doped GaSe monolayer, *Phys. Lett. A* **382**, 667 (2018).
- [29] M. Hong, X. B. Zhou, J. P. Shi, Y. Qi, Z. P. Zhang, Q. Y. Fang, Y. G. Guo, Y. J. Sun, Z. F. Liu, Y. C. Li, Q. Wang, and Y. F. Zhang, Quasi-freestanding, striped WS<sub>2</sub> monolayer with an invariable band gap on Au(001), *Nano Res.* **10**, 3875 (2017).
- [30] See the Supplemental Material at <http://link.aps.org/supplemental/10.1103/PhysRevApplied.13.024003> for bias-voltage-dependent STM images of the Co/WS<sub>2</sub> systems; stability of the Co QDs at room temperature, excluding the effect of point defects; possible geometrical structures of Co<sub>N</sub>/WS<sub>2</sub> systems, and other possible QD structures.
- [31] M. Y. Lai and Y. L. Wang, Direct Observation of two Dimensional Magic Clusters, *Phys. Rev. Lett.* **81**, 164 (1998).
- [32] Y.-P. Chiu, C.-M. Wei, and C.-S. Chang, Density functional study of surface-supported planar magic Ag nanoclusters, *Phys. Rev. B* **78**, 115402 (2008).
- [33] Y.-P. Chiu, L.-W. Huang, C.-M. Wei, C.-S. Chang, and T.-T. Tsong, Magic Numbers of Atoms in Surface-Supported Planar Clusters, *Phys. Rev. Lett.* **97**, 165504 (2006).
- [34] J. Tersoff and D. R. Hamann, Theory of the scanning tunneling microscope, *Phys. Rev. B* **31**, 805 (1985).
- [35] H. Murata, K. Kataoka, and A. Koma, Scanning tunneling microscope images of locally modulated structures in layered materials, MoS<sub>2</sub>(0001) and MoSe<sub>2</sub>(0001), induced by impurity atoms, *Surf. Sci.* **478**, 131 (2001).
- [36] H. Kwon, K. Lee, J. Heo, Y. Oh, H. Lee, S. Appalakondiah, W. Ko, H. W. Kim, J. W. Jung, H. Suh, H. Min, I. Jeon, E. Hwang, and S. Hwang, Characterization of edge contact: Atomically resolved semiconductor–metal lateral boundary in MoS<sub>2</sub>, *Adv. Mater.* **29**, 170293 (2017).
- [37] M. Seol, S. Kim, Y. Cho, K. E. Byun, H. Kim, J. Kim, S. K. Kim, S. W. Kim, H. J. Shin, and S. Park, Triboelectric series of 2D layered materials, *Adv. Mater.* **30**, 1801210 (2018).
- [38] C. J. Zhou, W. H. Yang, Y. P. Wu, and W. Lin, Metal-atom-induced charge redistributions and their effects on the electrical contacts to WS<sub>2</sub> monolayers, *Phys. Status Solidi B* **252**, 1783 (2015).
- [39] P. Igor, S. Gotthard, and T. David, Designing Electrical Contacts to MoS<sub>2</sub> Monolayers: A Computational Study, *Phys. Rev. Lett.* **108**, 156802 (2012).